ISSN 1995-0780, Nanotechnologies in Russia, 2016, Vol. 11, Nos. 1–2, pp. 41–56. © Pleiades Publishing, Ltd., 2016.
Original Russian Text © L.N. Obolenskaya, A.A. Gaynanova, G.V. Kravchenko, G.M. Kuz'micheva, E.V. Savinkina, E.N. Domoroshchina, A.M. Tsybinsky, A.V. Podbelsky, 2016, published in Rossiiskie Nanotekhnologii, 2016, Vol. 11, Nos. 1–2.

Nanocomposites Based on Silicon Dioxide of Different Nature with Functional Titanium Dioxide Nanoparticles

L. N. Obolenskaya[a], A. A. Gaynanova[a], G. V. Kravchenko[a], G. M. Kuz'micheva[a], E. V. Savinkina[a], E. N. Domoroshchina[a], A. M. Tsybinsky[b], and A. V. Podbelsky[c]

[a] *Federal State Budget Educational Institution of Higher Education "Moscow Technological University", pr. Vernadskogo 86, Moscow, 119571 Russia*

[b] *Fedorovsky All-Russia Research Institute of Mineral Raw Materials, Staromonetnyi per. 31, Moscow, 119017 Russia*

[c] *National Research University Higher School of Economics, ul. Myasnitskaya 20, Moscow, 101000 Russia*

e-mail: galina_kuzmicheva@list.ru

Received February 19, 2015; in final form, October 15, 2015

Abstract—Nanocomposites TiO_2/SiO_2 with photocatalytic and adsorptive properties were prepared by co-dispersing of η-modification and anatase (commercial Hombifine N) and SiO_2 (opal, granules, ultrafine) in ethanol (or ethanol–water mixture in the presence of chlorophylls or porphyrins) with ultrasonic treatments of the mixture (method 1) and an aqueous solution of KOH with a microwave treatment (method 2), as well as the introduction of SiO_2 in the reaction mixture during the synthesis of TiO_2 by brief hydrolysis of sulfate titanyl (method 3). It was found that the state of titania in the sample (X-ray amorphous or nanocrystalline) and its deposition on SiO_2 nanocomposites depend on the method and the conditions of obtaining. It was established that the photocatalytic activity of nanocomposite TiO_2/SiO_2 (granules) (method 1) photosensitized by coproporphyrin I in the visible range and the photocatalytic activity of nanocomposite TiO_2/SiO_2 (opal) (method 3) in the near UV range exceed activity of the commercial sample of $TiSiO_4$ by more than 20-fold and ~7-fold, respectively. It was shown that the nanocomposite TiO_2/SiO_2 (opal) significantly reduces the concentration of cations (in particular, Be, Ni, Bi) in the model water systems.

DOI: 10.1134/S1995078016010110

INTRODUCTION

Nanocomposites are multiphase solid materials consisting of several components, wherein at least one of them has an average crystallite (particle) size in the nanoscale range (up to 100 nm). This determination can be used, in particular, for designation of solid combinations of massive matrix (carrier) and nanosized phase(s) (functional nanoparticles, reinforcing phase), which differ in their properties because of the differences in the structure and physicochemical properties. Mechanical, electrical, thermal, optical, electrochemical, catalytic, and other properties of nanocomposites differ from the properties of its components. Limitation in the scale for these effects is estimated as follows: <8 nm for (photo)catalytic activity, <10 nm for adsorption capacity, <20 nm for transferring hard magnetic material into soft, <50 nm for changing the refractive index, and <100 nm in order to achieve superparamagnetism, mechanical strength, or limiting changes in the structure of the composite.

In the formation of nanocomposites, either the properties of the matrix (carrier) to improve a number of physicochemical properties of the introduced therein functional nanoparticles can be used, or manifestation of synergism can be used—summing effect of the interaction of the properties of matrix and nanoparticles significantly superior to the effect of each individual component in the form of their simple sum. In this regard, promising are TiO_2/SiO_2 nanocomposites, where the components are amorphous silica matrix (carrier) and nanocrystalline titanium dioxide (functional nanoparticles).

Amorphous silica is characterized by thermal stability and high surface area. The silicon atoms on the surface of SiO_2 nanoparticles of any nature differ in the properties (in particular, crystal-chemical and chemical) of the same atoms in bulk, where each silicon atom is connected to four oxygen atoms: surface silicon atoms contain free bonds, which are saturated by hydroxyl OH groups, which determines the hydrophility and sorption properties of SiO_2. Silanol groups (Si-OH) of silica in strength are comparable with acetic acid ($pK_a \sim 6$), and for some SiO_2 brands, they are even stronger [1]. They play a key role in modifying the silica, the role of which is performed in this case by titanium dioxide nanoparticles.

The manifestation of the properties of nanoparticles of titanium dioxide (photocatalyst, adsorption, bactericidal, and others) is caused by the formation of surface hydroxyl groups with high reactivity upon

Fig. 1. View of initial SiO_2 carriers: granules—GR (a), opal—OP (b), ultrafine (Aeroxide)—UF (c).

decreasing the crystallite size to 100 Å or less, moreover crucially, so that the amount of such crystallites in the sample is close to 100% (approaching a unimodal particle size distribution) [2, 3]. These groups are self-generated upon contact with electrolytes on semiconductors with a large bandgap (ΔE = 3.1–3.4 eV for nano-scaled titanium dioxide), resulting in high adsorbing capacity of the surface of titanium dioxide nanoparticles [2–8].

Irradiation of the semiconductor of titanium dioxide with light with excitation energy above the bandgap energy of the material results in the absorption of photons (hν) and transfer of electrons (e^-) from the valence band (VB) to the conduction band (CB), thus generating a positively charged hole (h^+) in the valence band. The electron-hole charge carriers ($h^+_{VB} + e^-_{CB}$), in turn, can recombine and dissipate the excess energy by a radiationless mechanism: *semiconductor* + $h\nu \rightarrow h^+_{VB} + e^-_{CB}$; $e^-_{CB} + h^+_{VB} \rightarrow$ *energy*, which reduces the overall efficiency of the photoexcitation process. The charge carriers not subjected to annihilation can migrate to the catalyst surface and initiate secondary reactions with the surface of adsorbed materials. The photoexcited electrons in the conduction band (CB) can react with oxygen to form superoxide or hydroperoxide radicals $e^-_{CB} + O_2 \rightarrow \cdot O_2^-$, and these reactive forms of oxygen can be involved in the decomposition of organic contaminants. Positively charged holes (h^+) in the valence band (VB) can generate hydroxyl radicals: $h^+_{VB} + H_2O \rightarrow \cdot OH + H^+$, which, in turn, oxidize the organic pollutants; in addition, ·OH radicals are formed under UV exposure, which play active role in photocatalytic activity [9, 10].

Titanium dioxide is widely used as a coating that is applied to porous oxide matrices of SiO_2 to increase its specific surface area and mechanical and thermal strength and to increase the selectivity of catalysts obtained on its basis [11–13]. In the literature, TiO_2/SiO_2 composites are described, which may be used as photocatalysts [14], solar energy converters [15], and key components to create self-cleaning surfaces [16].

The purpose of this work is to obtain, study, and compare the properties of TiO_2/SiO_2 nanocomposites with nanocrystalline titanium dioxide on the basis of silica of different nature.

OBJECTS AND METHODS OF STUDY

The objects of study are TiO_2/SiO_2 nanocomposites, for which silica served as a carrier: granules—GR; opal—OP (sample provided by Prof. M.I. Samoilovich); and ultrafine SiO_2 (Aeroxide)—UF (Fig. 1).

Table 1. Preparation of titanium dioxide samples

Sample	Initial reagent/mass, g	Volume of water, mL	Temperature, °C/duration, min	Coagulant/concentration, mol L^{-1}/volume, mL
TiO_2-1	$TiOSO_4 \cdot xH_2SO_4 \cdot yH_2O$/7.35	40	90/9	HCl/8.8/54
TiO_2-2	$TiOSO_4 \cdot xH_2SO_4 \cdot yH_2O$/7.35	20	80/44	HCl/8.8/54
TiO_2-3	$TiOSO_4 \cdot xH_2SO_4 \cdot yH_2O$/7.35	40	89/11	KCl/8.8/30
TiO_2-4	$TiOSO_4 \cdot 2H_2O$/4.32	42[1]	89/44	Cs_2SO_4/0.7/30[2]
TiO_2-5	$TiOSO_4 \cdot xH_2SO_4 \cdot yH_2O$/7.35	40	75/8	KCl/8.8/40[3]

[1]4.7 M aqueous solution of H_2SO_4 was taken instead of water.
[2]After adding the coagulant, the reaction mixture was stirred at room temperature for 45 min.
[3]Before adding coagulant, the reaction mixture was aged at room temperature for 30 days.

Table 2. Preparation of nanocomposites by method 3

Sample	Initial reagent/mass, g	Volume of water, mL	Heating temperature, °C/duration, min	Silica/mass, g
TiO_2/SiO_2(UF)	$TiOSO_4 \cdot xH_2SO_4 \cdot yH_2O$/7.35	40	91–97/8	Ultrafine/0.2
TiO_2/SiO_2(UF-1)	$TiOSO_4 \cdot xH_2SO_4 \cdot yH_2O$/7.35	40	95/12	Ultrafine/0.2
TiO_2/SiO_2(UF-2)	$TiOSO_4 \cdot xH_2SO_4 \cdot yH_2O$/7.35	40	95/45	Ultrafine/0.2
TiO_2/SiO_2(GR)	$TiOSO_4 \cdot 2H_2O$/1.80	50	87–93/39	Granulated/0.4
TiO_2/SiO_2(GR-1)	$TiOSO_4 \cdot xH_2SO_4 \cdot yH_2O$/7.35	20	77–83/5	Granulated/3[1]
TiO_2/SiO_2(OP)	$TiOSO_4 \cdot xH_2SO_4 \cdot yH_2O$/7.35	40	87–93/9	Opal/0.53[2]
TiO_2/SiO_2(OP-1)	$TiOSO_4 \cdot xH_2SO_4 \cdot yH_2O$/7.35	40	95/15	Opal/0.53[3]

[1] Addition of 100 mL of water, holding at 80 °C for 39 min.
[2] Addition of 54 mL 8.8 M hydrochloric acid.
[3] Addition of 34 mL 8.8 M hydrochloric acid.

Samples with titanium dioxide (Table 1) used for the production of composites and/or as a reference sample were obtained by hydrolysis of titanyl sulfate followed by separation of the product by vacuum filtration (overnight), washing with water and acetone, and drying at 90°C (starting reagents are $TiOSO_4 \cdot xH_2SO_4 \cdot yH_2O$ (Aldrich, CAS no. 123334-00-9) or $TiOSO_4 \cdot 2H_2O$ (Aldrich, CAS no. 13825-74-6)). In addition, commercial samples of Hombifine N and "$TiSiO_4$" (Aldrich, MDL no. MFCD00799909) were used.

Method 1. Composites were synthesized by joint dispersal of the samples with titanium dioxide and silica in ethanol or ethanol–water mixture in the presence of porphyrins.

The sample of TiO_2-3/SiO_2(GR-2) was obtained by dispersal of 0.4 g of TiO_2-3 in ethanol followed by the introduction of coproporphyrin I tetraisopropyl ester (0.0058 g) using ultrasound (20 min), addition of 10 mL of 1 M NaOH, stirring (15 min), and introduction of 0.1 g of granular silica. The resulting solid phase a day later was separated by vacuum filtration, washed with water and acetone, and dried at 90°C.

The sample of TiO_2-4/SiO_2 (UF-Chl) was obtained by co-dispersion of 0.34 g of SiO_2 (UF) and 0.06 g of TiO_2-4 in a water–ethanol mixture (2 : 1 by volume) in the presence of chlorophyll A (CAS no. 479-61-8) and B (CAS no. 519-62-01) (total weight is 50 mg) followed by sonication (5 min). The resulting solid phase a day later was separated by vacuum filtration, washed with water and acetone, and dried in air, and then ground in a porcelain mortar.

Method 2: Composites were obtained by co-dispersion of nano-TiO_2 and SiO_2 in an aqueous solution of KOH with microwave (MW) treatment.

Samples of TiO_2-5/SiO_2 (OP), TiO_2-5/SiO_2 (UF), Hombifine N/SiO_2(UF), and Hombifine N/SiO_2(OP) were prepared by dispersion of 0.3 g TiO_2-5 or Hombifine N and 0.1 g of SiO_2 (OP, UF) in 40 mL of 0.1 M aqueous solution of KOH, followed by microwave (MW) treatment of the obtained dispersions for 30 min at room temperature. The resulting solid phase was separated by vacuum filtration, washed with water and acetone, and dried at 90°C.

Method 3: Composites were synthesized by introducing silica into the reaction mixture during the synthesis of titanium dioxide by brief hydrolysis of titanyl sulfate (Table 2). After further treatment (in some cases), the resulting solid phase a day later was separated by vacuum filtration, washed with water and acetone, and dried at 90°C. As reference samples in the study of the photocatalytic activity (PCA), TiO_2-1 and TiO_2-2 samples not containing SiO_2 were obtained, so before introduction of SiO_2 to the reaction mixture (TiO_2/H_2SO_4 sol), part of the reaction mixture was separated and TiO_2 was precipitated from it in the absence of SiO_2 (Table 1).

X-ray survey of the samples with rotation was performed on an HZG-4 diffractometer (Ni-filter): CuK_α on the diffracted beam in continuous (1°C/min) or stepwise (dialing time of pulses of 10 s., step size of 0.02°, range of 2θ angles from 2° to 50°–80°) modes. The crystallite size were calculated (excluding possible microstrains) according to the formula $D = K\lambda/\beta\cos\theta$, where $\lambda = 1.54051$ Å is the wavelength (CuK_α), $2\theta \sim 25°$ for TiO_2 and $2\theta \sim 22°$ for SiO_2 (θ is the scattering angle), β is the integral width of the peak, and the particle shape factor (Scherrer ratio) K was taken to be 0.9. The standard deviation is ±5%.

Study of the microstructure of TiO_2/SiO_2 nanocomposite (OP) was performed by scanning electron microscopy (SEM) using a JSM 7500F high resolution electron microscope. Chemical qualitative and quantitative composition was determined by X-ray microanalysis (XRMA) at three points, using an energy dispersive X-ray microanalyzer, established in the same high-vacuum chamber of the microscope. Quantita-

tive analysis was performed using the INCA Penta FET mathematical program for all elements with atomic number >3. The limit of repeatability of the results was 0.1% [17]. For the analysis of photographs obtained by SEM, the authors developed a specialized program. Its purpose was automatization of the isolation process on the photograph of spherical contours of the images of particles and construction of the histogram of particle size distribution. The program was written in the C# language and oriented on Net Framework platform versions 3.5 and above. The initial data for the program are the image of micrographs and particle size range upon the construction of the histogram. Processing (counting) of the photograph begins with automatic recognition of the spherical contours of particles. To select the borders of images in the program, the Canny operator is used [18], supplemented by the reduction filter of the boundaries to a spherical shape. Owing to the fact that the automatic marking of the contours of particles for "bad" (noisy) photos gives unsatisfactory results, the program includes a visual check of the results of automatic selection of boundaries and manual dialogue adjustment of marking boundaries. In addition, the program allows one to exclude the stage of automatic construction of boundaries and highlight spherical boundaries of particles manually. The procedure of such dialogue markup is partially automated.

Study of the adsorption capacity of the samples was performed on synthetic mixtures (ICP-MS-68A-A standard from High-Purity Standards, USA; the solution contains 48 elements in the concentration of 10 mg/L of each); 10 mL of standard solution with the concentration of 2 ppm ($C_{initial}$) ions in 0.4% nitric acid was added to the weighed portion of the sample with the mass of 30 mg. The solutions were shaken on a shaker for 3 h and then filtered through a 0.45 μm membrane filter. The concentration of metals in the solutions after sorption (C_{final}) was measured by inductively coupled plasma mass spectrometry (ICP-MS) (Agilent 7500c, USA). To optimize the performance of the instrument with respect to the sensitivity, mass resolution, and calibration of masses of elements being determined, Agilent Tuning Solution containing Li, Y, Ce, Tl, and Co (concentration of 10 μg/L) in 2% HNO_3 solution was used. The ratios of $^{140}Ce^{16}O^+/^{140}Ce^+$ ($^{137}Ba^{2+}/^{137}Ba^+$) were minimized to reduce the interferences from oxide ions (doubly charged ions). Such instrumental parameters as carrier gas flow, position of the burner, accelerating voltage, speed of the peristaltic pump, and integration parameters were optimized to achieve higher sensitivity and reduce the number of isobaric interferences. The maximum power delivered to the plasma was 1200 W. Matched argon flow rates were as follows: plasma forming—15 L/min, auxiliary—0.8 L/min, spray—1.4 L/min. For each mass (from 27 to 208 amu), 40 scans were used (50 ms) in triplicate. All results of ICP-MS analysis (construction of calibration straight lines, setting of the device using special solutions, statistical data, and concentrations of elements in solutions) were obtained using the ICP-MSTopAgilent software package.

Electronic absorption spectra of the samples were taken with an Akvilon SF 103 spectrophotometer.

Photocatalytic activity was studied on the model decomposition reaction of methyl orange organic dye (MeO, CAS no. 547-58-0). Discoloration of methyl orange was the standard model reaction allowing one to compare the activity of different photocatalysts. To the aqueous dye solution (initial concentration of 0.05 mmol/L) of pH ~ 3–4, powder of either nanocomposite or its starting components were added (mass content of 0.05 g/L). The resulting slurry (volume of 50 mL) was irradiated with light in the UV range of 250–400 nm (DRT irradiator—UVO-V-4, DRT 125 mercury lamp, irradiator power—125 W; Cam—Camelion UV lamp, 26 W) or in the visible range (Hal—halogen lamp, irradiation at wavelengths of ⩾450 nm, power of 250 W; Lum—energy saving reflector lamp with color temperature of 4200 K, which corresponds to the radiation maximum in the visible range of about 560–570 nm; power of 15 W (according to the amount of emitted light photons, it corresponds approximately to a 75 W halogen lamp) in an open container (the irradiation area of 0.07–0.09 m^2) at constant stirring using a magnetic stirrer for 150–240 min. Aliquots (10 mL) were taken from the reaction mixture and, if necessary, the solid phase was separated by centrifugation (OPn-8UKhL42 centrifuge).

Change in the concentration of MeO during the photoreaction (c/c_0 value) was controlled by changing the intensity of the absorption band of the chromophore group at $\lambda = 450$–470 nm. The used model photoreaction refers to reactions of a pseudo first order, for which the rate constant (k value) is calculated as the slope of the dependence of the change in the substrate concentration c/c_0 on the irradiation time τ in rectifying semilogarithmic coordinates (the accuracy of the linear approximation of kinetic curves on the R-factor in all cases is not less than 0.95; the error in determining the reaction rate constant is 10%).

RESULTS AND DISCUSSION

Characterization of Initial Samples and Nanocomposites

Figure 2 shows the diffraction patterns of the silica of different nature used in the present work.

Samples with ultrafine (UF) (Fig. 2a) and granular (GR) (Fig. 2b) SiO_2, in addition to amorphous silica, contain the impurity of amorphous hydrated silica (HS) of probable composition of $SiO_{2-x}(OH)_{2x} \cdot yH_2O$ (characteristic diffraction reflection at $2\theta \sim 11°$–$12°$) in different amounts (according to the ratio of the

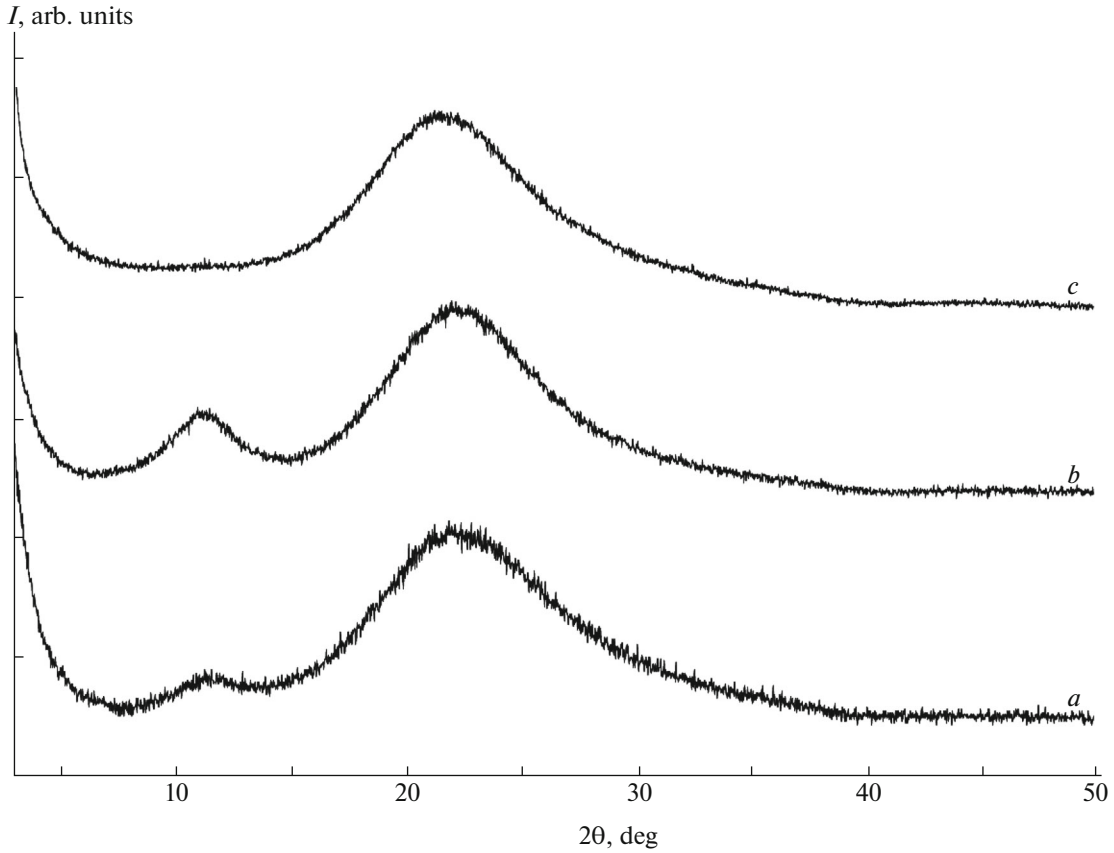

Fig. 2. Diffractograms of ultrafine SiO_2 (UF) (a), SiO_2 granules (GR) (b), and opal (OP) (c).

reflection intensity with 2θ ~ 11°–12°, in GR more than compared to UF). Sample with opal is single-phase (Fig. 2c).

In addition to the composition, samples with SiO_2 differ in the characteristics of the microstructure (lowest specific surface, determined by the comparative method [17], and the pore sizes for OP, and the largest for GR). The average crystallite sizes of them are about the same, a little more for granular (GR) SiO_2 (Table 3). In this case, the average crystallite size correlates with the content of HS in the composition of the samples: with the increase in the intensity ratio of

Table 3. Characteristics of silica

Characteristic	Opal[1]/Opal[2] (OP)	Ultrafine SiO_2 (Aeroxide)(UF)	SiO_2 granules (GR)
Composition of the samples according to X-ray diffraction (XRD)	SiO_2	SiO_2 + HD (8 : 1)	SiO_2 + HD (3 : 1)
The average crystallite size	42(2)	42(2)	45(2)
Specific surface by BET method (S_{BET}), m^2/g	10.1/11.8	294.2	257.9
Specific surface by comparative method (S_{CM}), m^2/g	10.1/10.7	180	330
Volume of ultrasmall nanopores (diameter of pores ⩽2 nm) (V_{UNP}), cm^3/g	–/0.003	0.076	0.069
Volume of nanopores (diameter of pores ⩽100 nm) (V_{NP}), cm^3/g	0.029/0.031	0.595	0.886

[1] Coarse.
[2] Crushed.

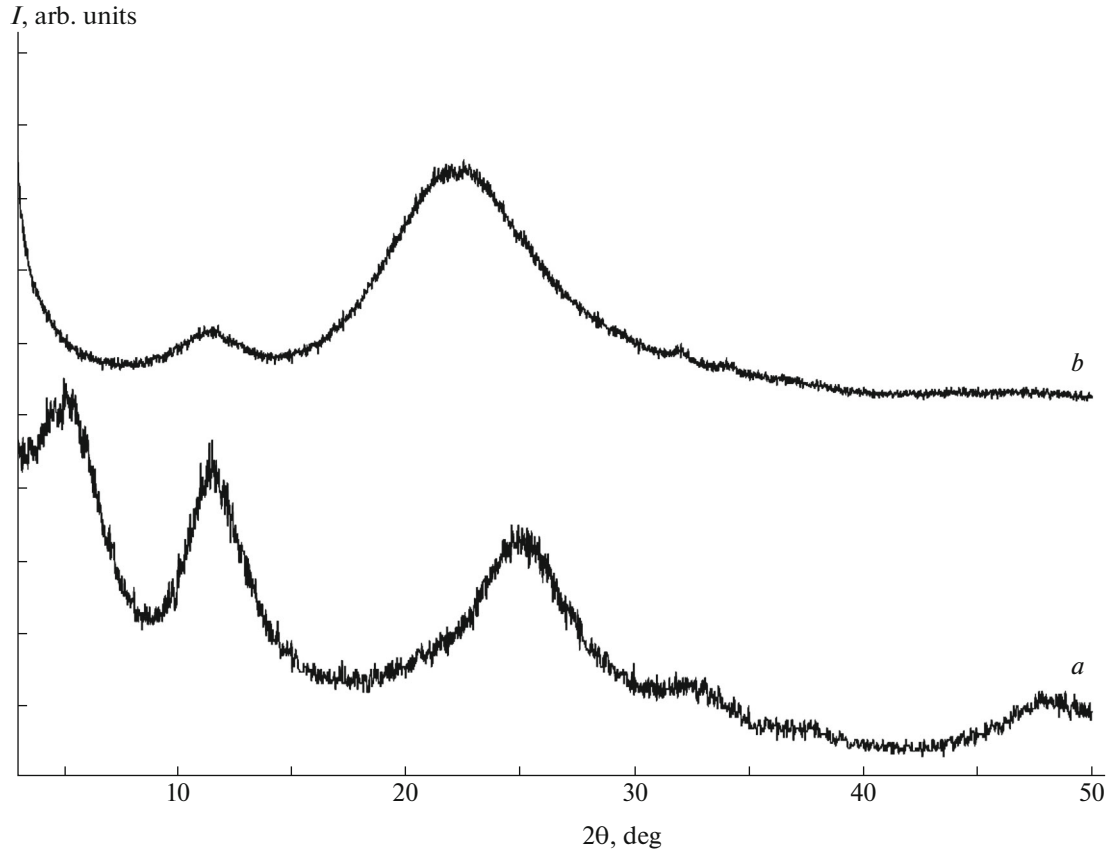

Fig. 3. Diffractogram of TiO_2-3 (a) and TiO_2-3/SiO_2 (GR) nanocomposite (b) (method 1).

diffraction reflections of SiO_2 : HS, which is proportional to SiO_2 and HS contents in the sample (Table 3), the average crystallite size (D value) of SiO_2 tends to decrease. This may indicate the impurity nature of HS in the samples with SiO_2, instead of depositing on the surface of the crystallites, which would cause an inverse relationship.

Samples Obtained by Method 1

Figure 3 shows the diffraction patterns of TiO_2-3 and TiO_2-3/SiO_2 (GR) nanocomposite obtained by joint dispersion of TiO_2-3 and granular silica in the presence of coproporphyrin I tetraisopropyl ester. Initial TiO_2-3 contains η-TiO_2 (characteristic diffraction reflections at 2θ ~ 4°–5° and ~ 33° [2]) and a large amount of hydrated titanium dioxide $TiO_{2-x}(OH)_{2x}\cdot yH_2O$ (HD). Nanocomposite TiO_2-3/SiO_2(GR) (Fig. 3b) also contains HD as does the source titanium dioxide (Fig. 3a), although its amount in the nanocomposite is much less (Table 4). The diffractogram of TiO_2-3/SiO_2(GR) does not contain diffraction reflections belonging to titanium dioxide (Fig. 3b), indicating either its small amount in the nanocomposite (below the sensitivity of this X-ray experiment) or its X-ray amorphism, which is more likely. The average crystallite size of SiO_2 for TiO_2-3/SiO_2(GR) (Table 4, Fig. 3b) is greater than that for the initial TiO_2-3.

Comparing the diffraction patterns of the TiO_2-4 sample (Fig. 4a) and TiO_2-4/SiO_2(UF-Chl) nanocomposite prepared by joint dispersion of SiO_2 (UF) and TiO_2-4 in the presence of chlorophylls (Fig. 4b) shows the opposite effect (Table 4). In turn, for TiO_2/SiO_2(UF-Chl) (Table 4, Fig. 4b), the mean crystallite sizes were greater (D = 47(2) Å) than for SiO_2(UF-Chl) (composition: SiO_2 + HS (1.5 : 1), D = 41(2) Å) (Fig. 4c), which is synthesized similarly to TiO_2/SiO_2(UF-Chl), but without the addition of titanium-containing components. Analyzing the data in Table 4, one can notice an inverse relationship between the size D and HD or HS content in the composition of the samples with η-TiO_2 or nanocomposites: the more HD or HS, the smaller the value D. This relationship indicates the presence of hydrated particles in the nanocomposites and nanoparticles of initial samples of TiO_2 on the surface, unlike the initial samples of SiO_2 of different nature (see above).

Table 4. Characteristics of the samples with TiO_2 and TiO_2/SiO_2 nanocomposites

Samples of TiO_2		
Sample/method of synthesis	Composition according to X-ray phase analysis	Size of crystallites D, Å
TiO_2-3	η-TiO_2 + HD (1 : 1) (Fig. 3a)	37(2)
TiO_2-4	η-TiO_2 + HD (2 : 1) (Fig. 4a)	50(3)
TiO_2-5	η-TiO_2 (Fig. 5a)	38(2)
Hombifine N	anatase (Fig. 6a)	81(4)
TiO_2-1	η-TiO_2 + HD (1.5 : 1)	47(2)
TiO_2-2	η-TiO_2 + HD (4 : 1)	55(3)
TiO_2/SiO_2 nanocomposites		
TiO_2-3/SiO_2(GR-2) / 1	SiO_2 + HD (5 : 1) (Fig. 3b)	44(2)
TiO_2-4/SiO_2(UF-Chl) / 1	SiO_2 + HS (3.5 : 1) (Fig.3c)	47(2)
TiO_2-5/SiO_2(UF) / 2	η-TiO_2[1] (Fig. 5b)	–
TiO_2-5/SiO_2(OP) / 2	η-TiO_2[1] (Fig. 5c)	–
HombifineN/SiO_2(UF) / 2	anatase (Fig. 6b)	77.2(4)
Hombifine N/SiO_2(OP) / 2	anatase + HS (8 : 1) (Fig. 6c)	60.0(3)
TiO_2/SiO_2(UF) / 3	SiO_2 (Fig. 7a)	52(3)
TiO_2/SiO_2(UF-1) / 3	SiO_2 + anatase + HD (or HS) (4 : 1)[3] (Fig. 7b)	40(2)/52(2)[2]
TiO_2/SiO_2(UF-2) / 3	Anatase (Fig. 7c)	–/58(3)[2]
TiO_2/SiO_2(GR) / 3	SiO_2 (Fig. 7a)	50(3)
TiO_2/SiO_2(GR-1) / 3	SiO_2 (Fig. 7b)	55(3)
TiO_2/SiO_2(OP) / 3	SiO_2 + HD (8 : 1) (Fig. 8a)	38(3)
TiO_2/SiO_2(OP-1) / 3	SiO_2 + anatase + HD (7 : 1)[3] (Fig. 8b)	–

[1] Strongly hydrated.
[2] D_{SiO_2}/D_{TiO_2}.
[3] In parentheses, the ratio of SiO_2 : HD or HS is given.

Samples Obtained by Method 2

Figure 5 shows the diffraction patterns of the initial sample of TiO_2-5 (Fig. 5a), containing η-TiO_2, and the TiO_2-5/SiO_2(UF) (Fig. 5b) and TiO_2-5/SiO_2(OP) (Fig. 5c) nanocomposites.

As can be seen from Figs. 5b and 5c, nanocomposites containing highly hydrated η-TiO_2 are obtained, as indicated by the blurred reflection in a large range of 2θ angles of ~24°–35°, while the nature of the initial silica does not affect the composition of nanocomposites and average crystallite size.

On the diffractogram of the commercial sample of Hombifine N (Fig. 6a) and nanocomposites of Hombifine N/SiO_2 (UF) and Hombifine N/SiO_2 (OP) (Figs. 6b, 6c; Table 4), diffraction reflections are present (2θ ~ 25°, ~38°, ~48°), belonging to anatase (JCPDS 89-4921), and in Hombifine N/SiO_2 (UF), HD/HS is found (Table 4, Fig. 6b) as in the original UF (Fig. 2a). Diffraction peaks belonging to SiO_2 are absent in the diffractograms.

The average size of crystallites of anatase in Hombifine N/SiO_2 is less than that in the initial Hombifine N (Table 4), while in this case the presence of HD or HS in the composition of the samples decreases the size of crystallites.

Thus, the dispersion medium of initial dioxides of silicon and titanium and the processing method of the reaction mixture have a significant effect on the composition of the resulting nanocomposites: upon using method 1, nanocomposites contain X-ray amorphous titanium dioxide, and method 2 promotes the formation of nanocrystalline titanium dioxide.

Samples Obtained by Method 3

Upon the preparation of nanocomposites based on ultrafine (UF) silica (Fig. 7), an increase in the duration of heating of the reaction mixture (Table 4) leads to an increase in the content of nano titanium dioxide in their composition: only SiO_2 is present in TiO_2/SiO_2 (UF) (although an asymmetry of the peak

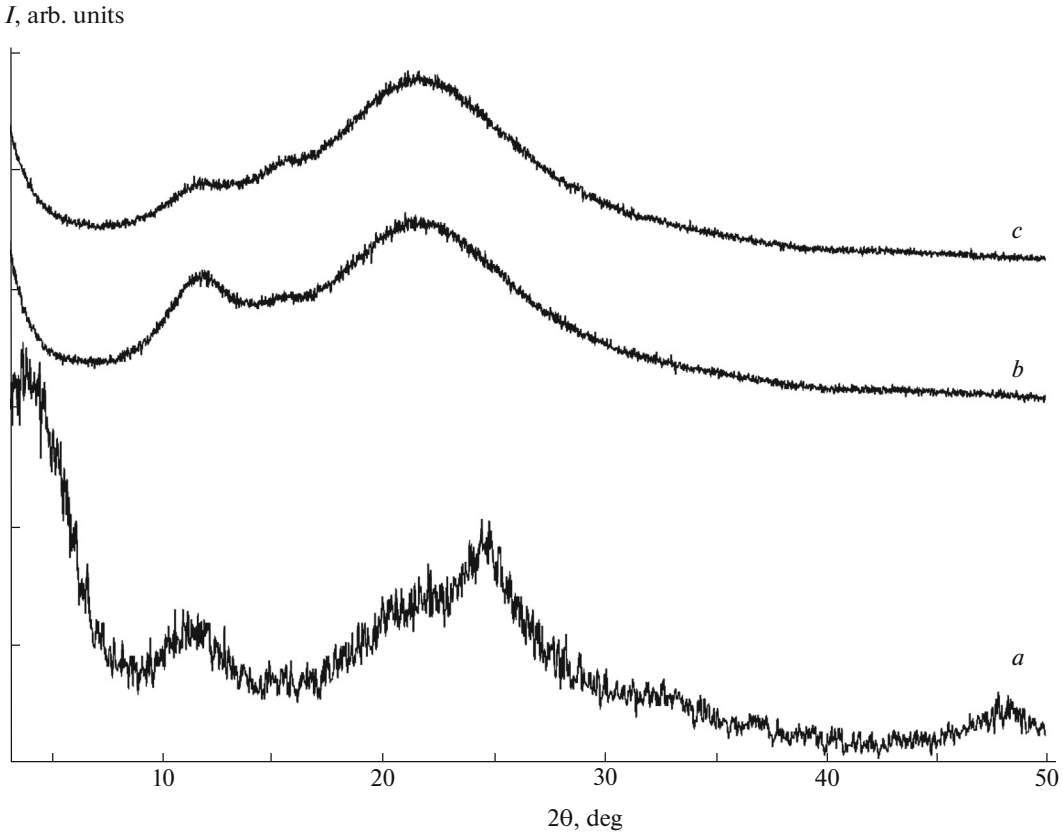

Fig. 4. Diffractogram of TiO_2-4 (a), TiO_2-4/SiO_2 (UF-Chl) nanocomposite (b) (method 1), and reference sample of SiO_2 (UF-Chl) (c).

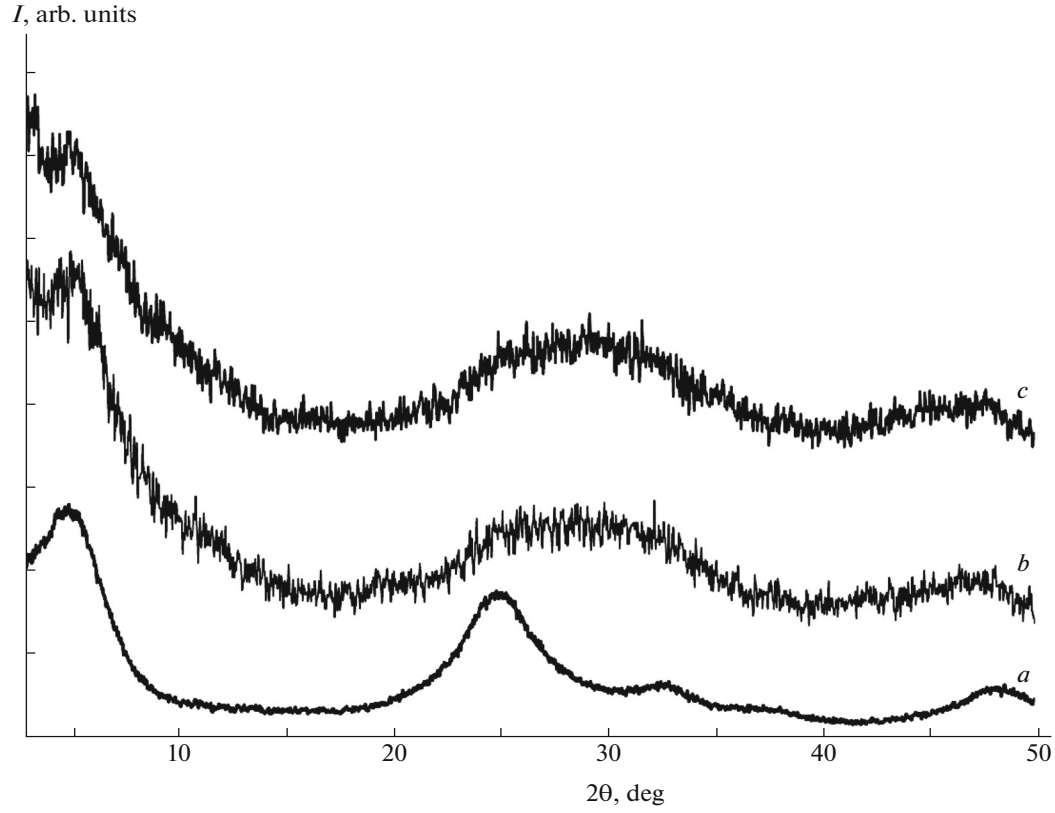

Fig. 5. Diffractograms of TiO_2-5 precursor (a) and TiO_2-5/SiO_2 (UF) nanocomposites (b) and TiO_2-5/SiO_2 (OP) (c) (method 2).

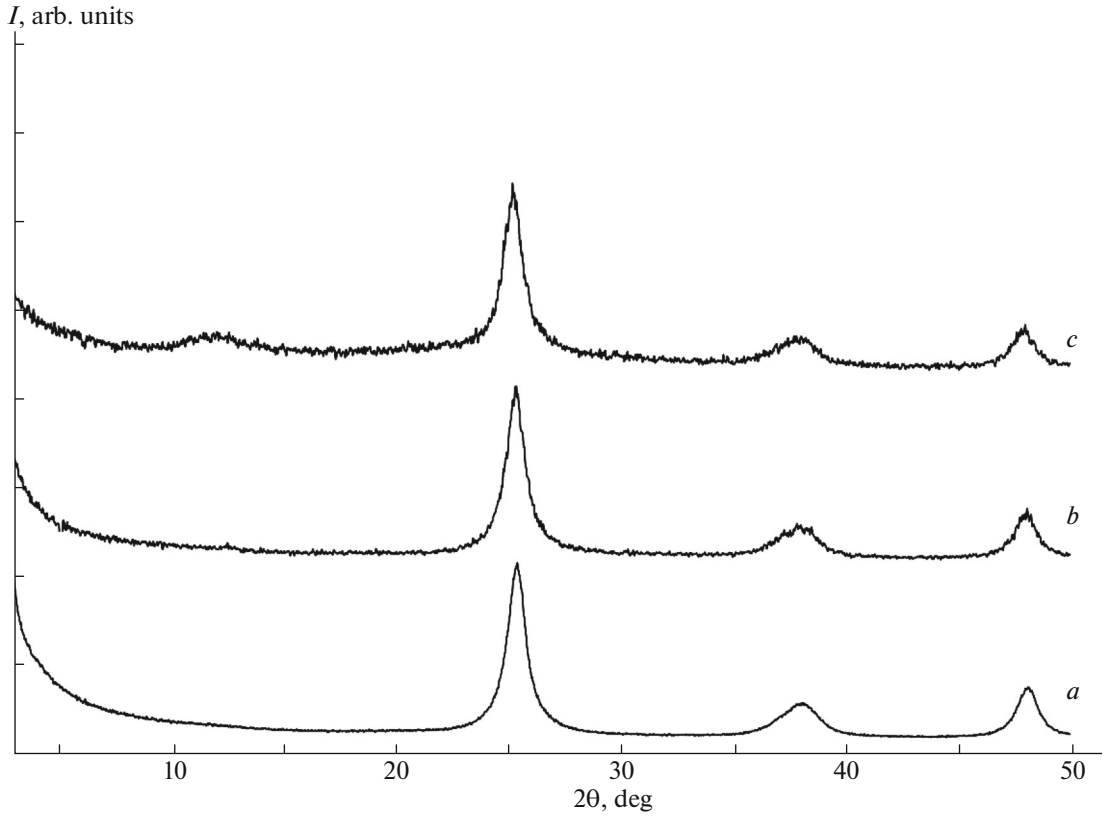

Fig. 6. Diffractograms of the initial sample of Hombifine N (precursor) (a) and nanocomposites of Hombifine N/SiO_2 (UF) (b) and Hombifine N/SiO_2 (OP) (c) (method 2).

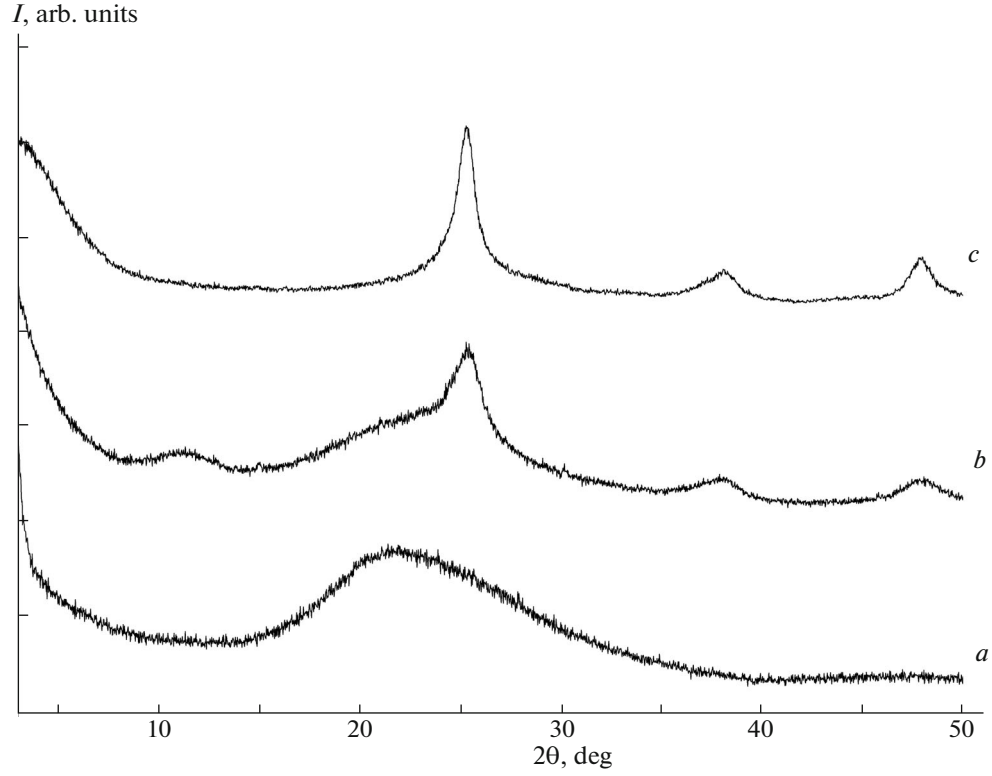

Fig. 7. Diffractograms of TiO_2/SiO_2 (UF) nanocomposites (a), TiO_2/SiO_2 (UF-1) (b), TiO_2/SiO_2 (UF-2) (c) (method 3).

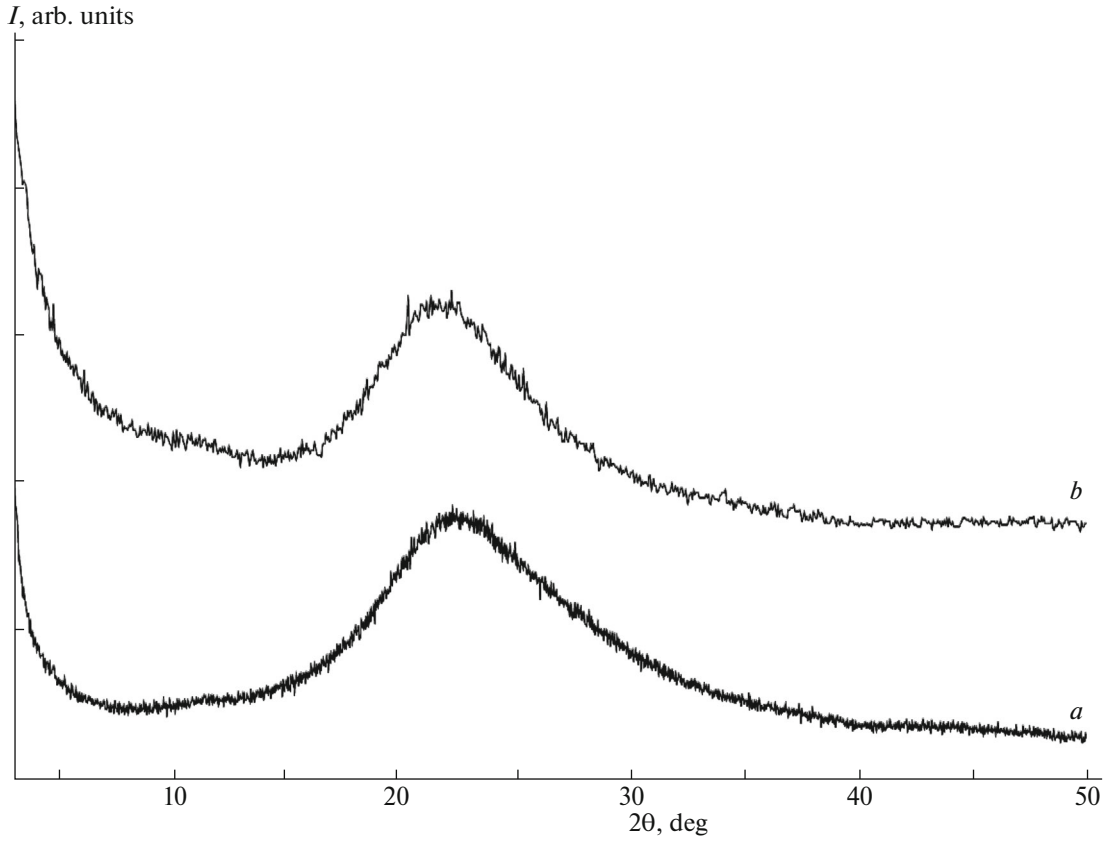

Fig. 8. Diffractogram of TiO_2/SiO_2 (GR) (a) and TiO_2/SiO_2 (GR-1) (b) nanocomposites (method 3).

is observed with 2θ ~ 22° to higher angles, i.e., toward 2θ ~ 25° with 100% diffraction reflection for anatase) (Fig. 7a); in TiO_2/SiO_2 (UF-2), anatase and an amorphous phase are found together with silica (Fig. 7b); and in TiO_2/SiO_2 (UF-2), only TiO_2 is observed with the structure of anatase (Fig. 7c).

Reflections are detected on diffraction patterns of TiO_2/SiO_2 (GR) (Fig. 8a) and TiO_2/SiO_2 (GR-1) (Fig. 8b) nanocomposites corresponding to only silica (Table 4, Fig. 8) (probably, titanium dioxide is in the X-ray amorphous state). Increasing the duration of synthesis upon the preparation of nanocomposites based on opal promotes the phase transition X-ray amorphous–nanocrystalline anatase; the latter is absent in the composition of TiO_2/SiO_2 (OP) (Fig. 9a) and observed in the composition of TiO_2/SiO_2 (OP-1) (Fig. 9b).

At the same time, there is the same tendency in the variation of the average crystallite size in nanocomposites: a greater content of HS in the samples leads to a decrease in the average crystallite sizes in nanocomposites of TiO_2/SiO_2 (Table 4), which are larger than the initial matrices of SiO_2 (Table 3). This does not preclude the deposition of nanoparticles of titanium dioxide on the surface of the matrix.

Electronic absorption spectra (EAS) of the obtained samples differ little from the electronic absorption spectrum of titanium dioxide. Figure 10 as an example presents EAS of a TiO_2/SiO_2 (OP) sample.

Photocatalytic Properties

The samples obtained by method 1 are colored, so photocatalytic activity (PCA) in the visible region of the spectrum is expected for them. The samples obtained by methods 2 and 3 are colorless; i.e., they can display PCA only upon irradiation in the UV range.

Method 1

The samples of titanium dioxide used to obtain nanocomposites by method 1, TiO_2-3 and TiO_2-4, exhibit PCA in the UV region of the spectrum with k = 0.024 and 0.022 min^{-1} (the source of radiation is DRT), respectively. In the visible range of the spectrum, they are not active. PCA of the samples were compared with the photoactivity of the commercial reference material ("$TiSiO_4$" powder), on the diffractogram of which (Fig. 11) amorphous reflexes can be seen, likely from HS (2θ ~ 11°–12°) and SiO_2 (2θ ~ 22°),

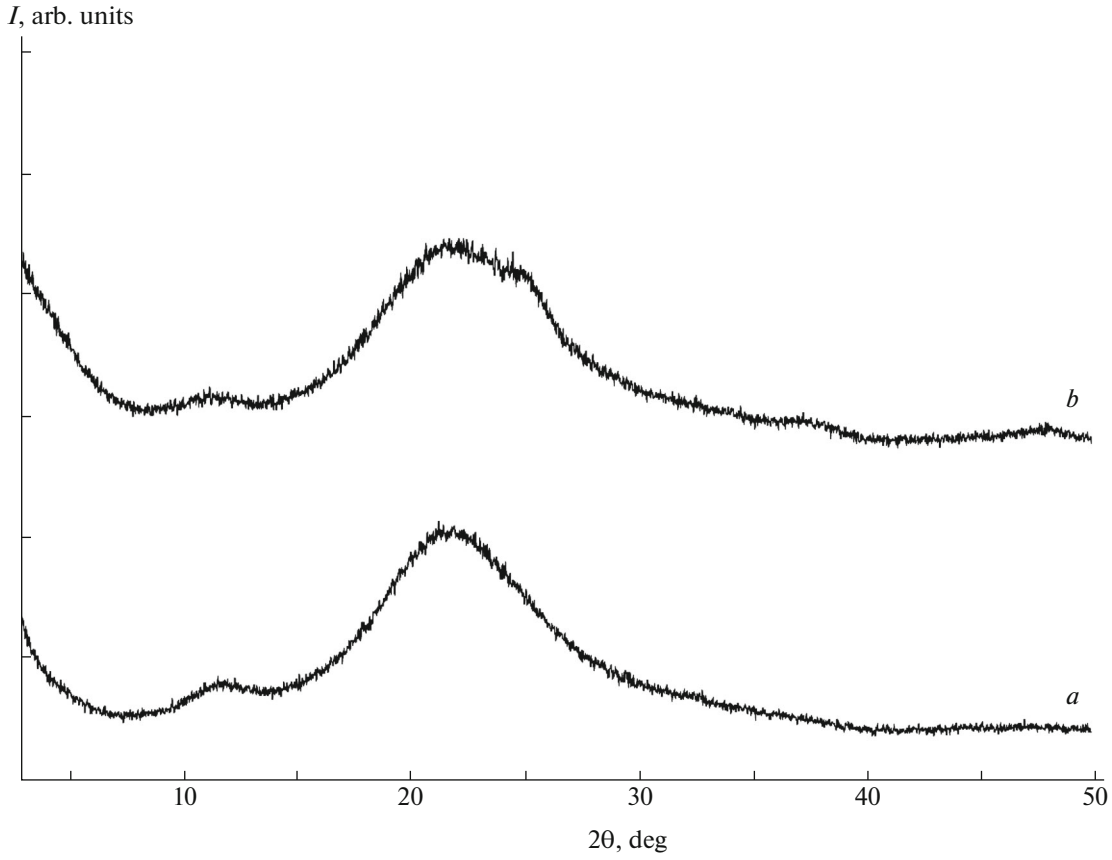

Fig. 9. Diffractogram of TiO_2/SiO_2 (OP) (a) and TiO_2/SiO_2 (OP-1) (b) nanocomposites (method 3).

as well as characteristic diffraction reflections for anatase with crystallite sizes (D = 160(3) Å) significantly higher than the similar dimensions of nano titanium dioxides presented in this paper (Table 4).

To improve the activity of TiO_2 in visible light, different ways are developed, and sensitization by dyes is considered a promising strategy for activating TiO_2 photocatalysis by visible light [9]. The process involves the absorption of light (mainly visible) by an organic dye (or colored contaminant), known as a sensitizer, followed by injection of electrons from the excited molecule of the sensitizer to the conduction band of the semiconductor material. The obtained cation radicals can lead to a number of oxidative processes and formation of active oxygen forms, which leads to degradation of various organic contaminants [19–21] or dyes, in particular, MeO (the mechanism of the process is virtually unknown, but likely cleavage of nitrogen–nitrogen bond occurs in the first stage, which leads to the disappearance of the color).

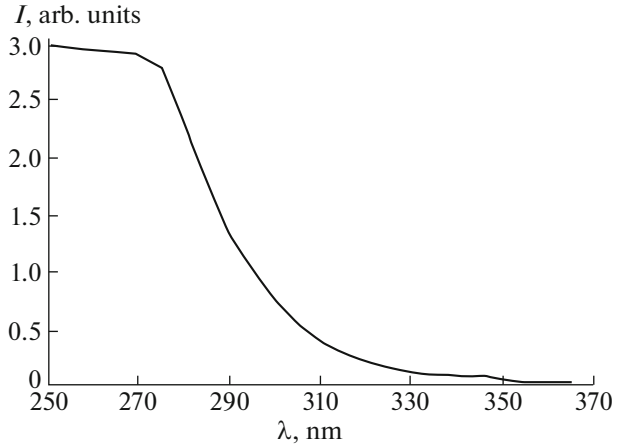

Fig. 10. EAS of TiO_2/SiO_2 (OP) sample suspended in water (ΔE_g = 3.61 eV).

In the visible range (radiation source is Hal), the activity of the TiO_2/SiO_2 (GR-2) sample photosensitized by coproporphyrin I obtained by method 1 exceeds the activity of the commercial reference sample of "$TiSiO_4$" under the same conditions more than 20-fold (Fig. 12). This indicates high efficiency of the sensitization of the composite by coproporphyrin I molecules.

The degree of concentration reduction of MeO due to its photodegradation (irradiation with Lum lamp) in the presence of SiO_2 (UF-Chl) nanocomposite not

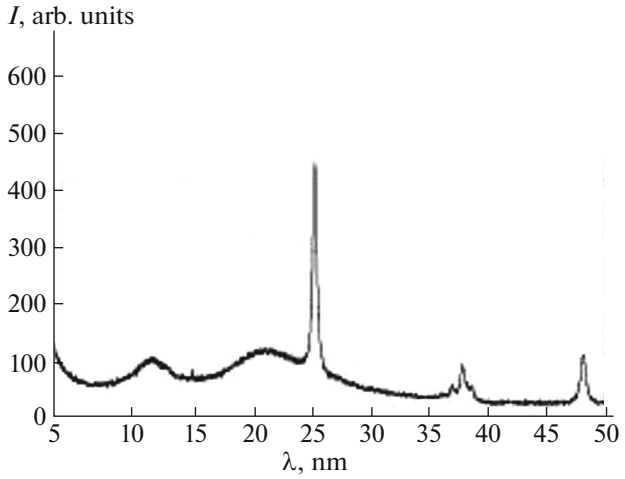

Fig. 11. Diffractogram of "$TiSiO_4$" (Aldrich; MDL no. MFCD00799909).

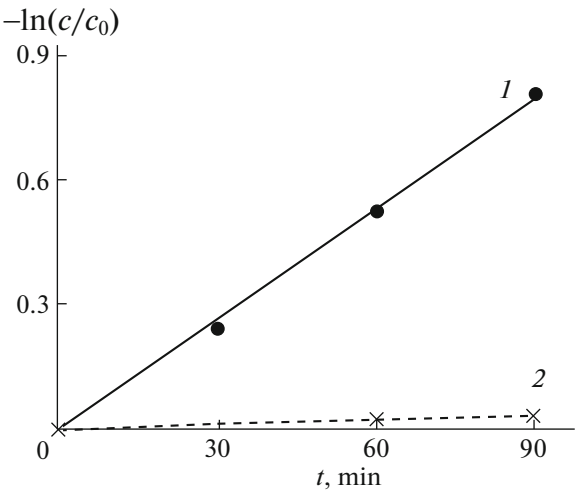

Fig. 12. Dependence of interpolated values of negative natural logarithm of the relative change in the concentration of MeO ($-\ln(c/c_0)$) on the duration (τ) of irradiation of photoreactivity mixture with light in the visible range (OSRAM halogen lamp, power of 250 W; temperature of 45–55°C) in the presence of the samples: (*1*) TiO_2/SiO_2 (GK-2) nanocomposite, sensitized by Coproporphyrin I (reaction rate constant $k = 0.0094$ min^{-1}); (*2*) reference sample of "$TiSiO_4$" (Aldrich) ($k = 0.0004$ min^{-1}).

containing titanium dioxide is equal to the degree of reduction of its concentration in the absence of light quanta (Table 5); i.e., the sample of SiO_2 (UF-Chl) does not manifest appreciable photocatalytic activity. It should be noted that, upon using "$TiSiO_4$" as a reference sample, reduction of the concentration of methyl orange (MeO) within the accuracy of the spectrophotometric method (0.1%) is not observed.

The rate of decrease in the concentration of MeO in the presence of TiO_2/SiO_2(UF-Chl) composite upon irradiation with visible light is ~15-fold more than in the presence of SiO_2(UF-Chl) (Fig. 13). It significantly exceeds the rate of decrease in the concentration of MeO in the dark, which indicates relatively high photocatalytic activity of TiO_2/SiO_2(UF-Chl). At the same time, the recovery rate of MeO by the sample of TiO_2/SiO_2(UF-Chl) in the dark exceeds the corresponding value for the sample of SiO_2(UF-Chl) ~3-fold (Table 5). This suggests that the introduction of the titanium oxide component to SiO_2(UF-Chl) leads not only to the appearance of the photocatalytic activity for it but also to the increase in its sorptive capacity with respect to MeO.

Method 2

Upon the model photocatalytic decomposition reaction of methyl orange dye in the UV range (source power is 26 W, irradiation time is 4 h), it was shown that the application of commercial titanium dioxide of Hombifine N grade on opal or ultrafine (UF) silica by method 2 results in a decrease in photocatalytic activity (Fig. 7, $k = 0.005$, 0.002, and 0.003 min^{-1}, respectively). Application of TiO_2-5 obtained in this paper on Opal (OP) and ultrafine (UF) silica gives the samples with even lower photocatalytic activity (Fig. 7). Thus, method 2 does not allow obtaining nanocomposites that are effective photocatalysts.

Method 3

Obtaining photocatalytic active nanocomposites based on ultrafine (UF) silica by method 3 is more promising than by method 2. Thus, the sample of TiO_2/SiO_2 (UF-1) is characterized by higher PCA than Hombifine N (Fig. 14).

It should be noted that increasing the synthesis time upon the preparation of nanocomposites based

Table 5. Decrease in the concentration of MeO (%) after 3 h of stirring of its solution with the samples modified by the mixture of chlorophyll A and B (Table 1)

Irradiation conditions Sample	In the absence of light quanta	Upon irradiation by fluorescent lamp (power of 15 W)
SiO_2(UF-Chl)	0.4	0.4
TiO_2/SiO_2(UF-Chl)	1.4	14.7

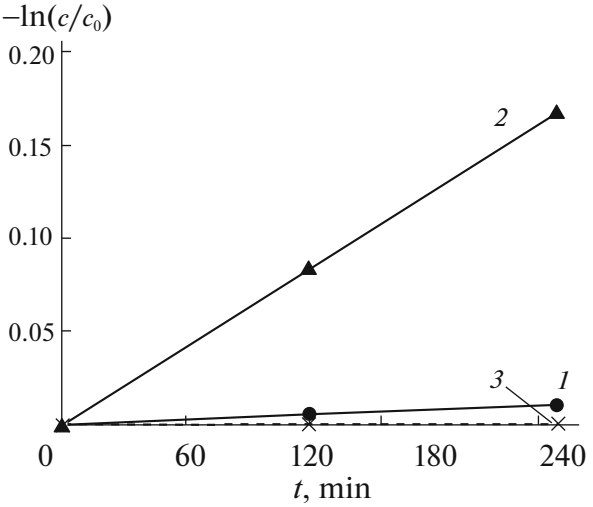

Fig. 13. Dependence of interpolated values of negative natural logarithm of the relative change in the concentration of MeO ($-\ln(c/c_0)$) on the duration (τ) of irradiation of photoreactivity mixture with light in the visible range (Camelion energy-saving lamp, power of 15 W; temperature of 20–30°C) in the presence of the samples: (*1*) SiO_2 (UF-Chl) (reaction rate constant $k = 0.00003$ min^{-1}); (*2*) TiO_2/SiO_2 nanocomposite (UF-Chl) ($k = 0.0007$ min^{-1}); (*3*) reference sample of "$TiSiO_4$" (Aldrich) (MeO concentration remains constant).

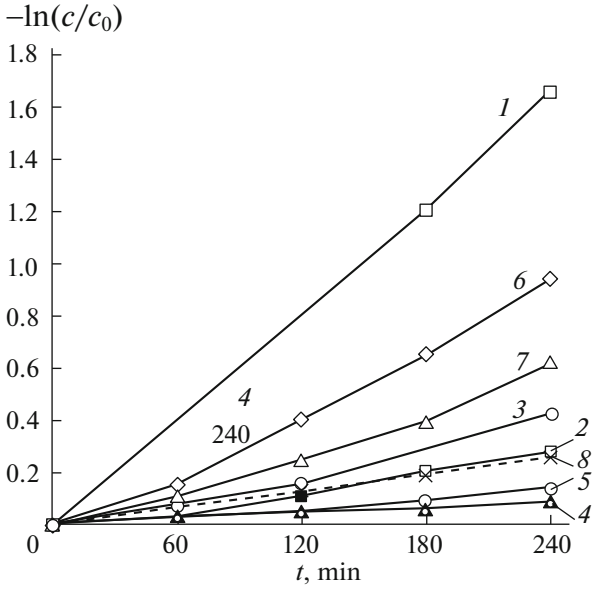

Fig. 14. Dependence of interpolated values of negative natural logarithm of the relative change in the concentration of MeO ($-\ln(c/c_0)$) on the duration (τ) of irradiation of photoreactivity mixture with light in UV range (Camelion energy-saving lamp, power of 26 W; temperature of 30–40°C) in the presence of the samples: (*1*) TiO_2/SiO_2(UF-1) ($k = 0.006$ min^{-1}); (*2*) TiO_2/SiO_2(UF-2) ($k = 0.0008$ min^{-1}); (*3*) TiO_2/SiO_2(OP-1) ($k = 0.001$ min^{-1}); (*4*) TiO_2-5/SiO_2(UF) ($k = 0.0004$ min^{-1}); (*5*) TiO_2-5/SiO_2(OP) ($k = 0.0006$ min^{-1}); (*6*) Hombifine N/SiO_2(UF) ($k = 0.003$ min^{-1}); (*7*) Hombifine N/SiO_2(OP) ($k = 0.002$ min^{-1}); (*8*) "$TiSiO_4$" reference sample (Aldrich) ($k = 0.001$ min^{-1}).

on ultrafine (UF) of silica reduces the photocatalytic activity (Fig. 14, curves *1* and *2* for TiO_2/SiO_2 (UF-1) and TiO_2/SiO_2(UF-2), respectively). It is possible that large differences in PCA of TiO_2/SiO_2(UF-1) and TiO_2/SiO_2(UF-2) nanocomposites (method 3) (Fig. 14) can be explained by the combined action of Si-OH and Ti-OH on the surface of nanoparticles in the case of TiO_2/SiO_2(UF-1) (Fig. 7).

With reduction of the synthesis time by method 3, the photocatalytic activity of the nanocomposite based on ultrafine (UF) silica exceeds the activity of Hombifine N to a greater degree (Fig. 15, curve *2*): $k = 0.017$ and 0.028 min^{-1} for Hombifine N and TiO_2/SiO_2 (UF), respectively (radiation source is DRT). Thus, the synthesis time of such samples should be minimized.

Method 3 allows also obtaining more active photocatalysts as compared with method 2 if opal (OP) is used as a carrier. The sample of TiO_2/SiO_2 (OP) (Fig. 15, curve *1*) shows greater activity than Hombifine N, $TiSiO_4$, and titanium dioxide obtained under similar conditions without adding silica: $k = 0.057$, 0.017, 0.008, and 0.019 min^{-1}, respectively (radiation source is DRT). However, with slightly increasing temperature and duration of the synthesis, PCA of the nanocomposite significantly decreases and becomes less than that for the reference samples (Fig. 14, curve *3* for TiO_2/SiO_2 (OP-1)).

The application of titanium dioxide by method 3 on granules (GR) of titanium dioxide gives a less efficient photocatalyst than upon using opal (OP). Although the obtained sample of TiO_2/SiO_2 (GR-1) exceeds the industrial samples of Hombifine N and $TiSiO_4$ in photocatalytic activity, but is inferior to the sample of titanium dioxide TiO_2-2 obtained under same conditions, but without addition of silica: $k = 0.019$, 0.017, 0.008, and 0.031 min^{-1}, respectively (radiation source is DRT) (Fig. 15).

When comparing photocatalytic properties of TiO_2/SiO_2 composites on all three carriers upon irradiation in the near UV range (irradiation power is 125 W, temperature is about 60°C, irradiation time is 1–1.5 h), it was found that the activity of the TiO_2/SiO_2(OP) composite (Fig. 15, curve *1*) exceeds the activity (under same conditions) of the "$TiSiO_4$" commercial sample (Fig. 15, curve *4*) ~7-fold, a factor of two higher than the activity of the TiO_2/SiO_2(UF) composite (Fig. 15, curve *2*), which, in turn, is half as much as the activity of TiO_2/SiO_2(GR-1) (Fig. 15,

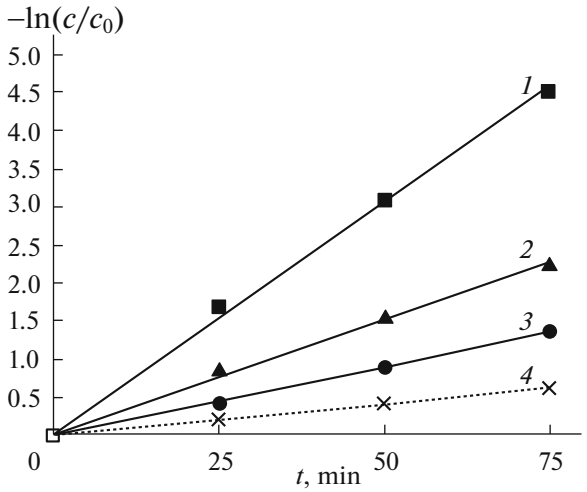

Fig. 15. Dependence of interpolated values of negative natural logarithm of the relative change in the concentration of MeO ($-\ln(c/c_0)$) on the duration (τ) of irradiation of photoreactivity mixture with light in UV range (DRT-125 mercury lamp, power of 125 W; temperature of 60–70°C) in the presence of the samples: (*1*) TiO_2/SiO_2 nanocomposite (OP) (k = 0.057 min^{-1}); (*2*) TiO_2/SiO_2 nanocomposite (UF) (k = 0.028 min^{-1}); (*3*) TiO_2/SiO_2 nanocomposite (GR-1) (k = 0.019 min^{-1}); (*8*) "$TiSiO_4$" reference sample (Aldrich) (k = 0.008 min^{-1}). TiO_2-1; k = 0.019 min^{-1}. TiO_2-2; k = 0.031 min^{-1}.

curve *3*). At lower lamp power and temperature of the photoreactivity mixture (irradiation power is 26 W, temperature is about 40°C), the most active is the nanocomposite with ultrafine (UF) SiO_2: PCA of TiO_2/SiO_2(UF-1) sample (Fig. 14, curve *1*) is sixfold higher than the activity of both the TiO_2/SiO_2(OP-1) sample (Fig. 14, curve *3*) and the reference sample of "$TiSiO_4$" (Fig. 14, curve *8*).

Table 6. Degree of sorption (R, %) of TiO_2/SiO_2 (OP) and TiO_2/SiO_2 (UF) nanocomposites obtained by method 3 (Table 1)

Element	R, %	
	TiO_2/SiO_2 (OP)	TiO_2/SiO_2 (UF)
Be	33.03	*
Mg	20.44	34.68
Co	31.44	*
Ni	34.78	*
In	25.57	*
Ce	25.36	*
Pb	26.83	*
Bi	36.56	*
Al	*	20.78
Ca	*	29.47

*Sorption degree R < 20%.

On kinetic curves of the photocatalytic decomposition reaction of MeO in the presence of all obtained nanocomposites of $TiO_2(TiO_2+HD)/SiO_2$ (upon irradiation both in the UV and in the visible range), the induction period characteristic of kinetic curves of MeO photodecomposition in the presence of the samples with η-modification, including with HD impurity, is absent [17, 22–24]. This can be explained by a higher value of the specific surface area of silicate carriers compared with the samples composed of only η-modification+HD [24].

Furthermore, as was stated in the introduction, pK_a of silanol surface groups is close to pK_a of acetic acid. During studies conducted in parallel, we found that namely this acid is the best solvent for the application of esterified coproporphyrins on TiO_2 [25]. Probably, namely the acidity of the medium created by acetic acid (pH ~ 3) and (locally) by surface silanol groups, on one hand, is sufficient to hydrolyze ester groups of the dye and, on the other hand, is not so great as to completely protonate carboxylate groups ($-COO^-$) of the dye after cleavage of isopropoxide groups from them. This promotes the binding of dye molecules to the surface of TiO_2 nanoparticles (deprotonated ligands form chelate complexes with titanium (IV) more actively than protonated ones). An indirect confirmation of this hypothesis is data on high photocatalytic activity of TiO_2/SiO_2 nanocomposites sensitized with zinc carboxyphenylporphyrinates [26].

Adsorption Properties

The sorption capacity of TiO_2/SiO_2 (OP) and TiO_2/SiO_2 (UF) nanocomposites is small: the greatest degree of extraction of Be, Ni, and Bi ions (R ~ 35%) and Mg ions (R ~ 35%) is found on TiO_2/SiO_2 (OP) and TiO_2/SiO_2 (UF) sorbents, respectively (Table 6). However, the degree of sorption of namely these ions on TiO_2/SiO_2 nanocomposites is greater than that on the samples with η-modification (R ~ 10%) doped with cations, for which the value of ion extraction of groups V–VI is >90% [27]. Probably, such sorption behavior of nanocomposites can be explained by the acidity of the medium (pH ~ 3–5), generated by locally surface silanol groups, which is greater (pH ~ 1–3) for nanoparticles with titanium dioxide.

Thus, as a result of the performed systematic work on obtaining TiO_2/SiO_2 nanocomposites in a variety of ways and radiographic characterization, TiO_2/SiO_2 (OP) nanocomposite is distinguished by its properties (PCA in the UV range, adsorption capacity), obtained by application of titanium dioxide to opal (CP) with the structure of η-modification with average crystallite size of D ~ 50 Å and spherical particles (associates)

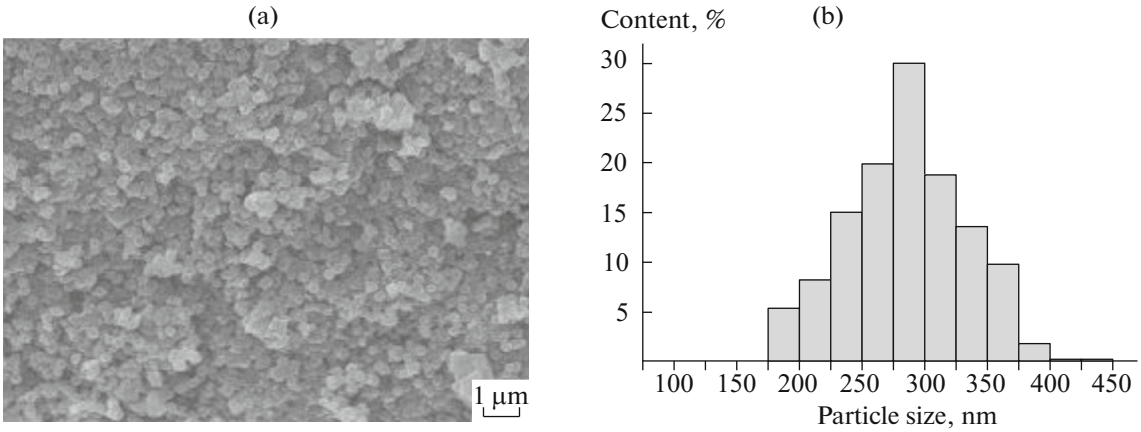

Fig. 16. Photographs of the microstructure of TiO_2/SiO_2 composite (OP) (a) and size distribution of TiO_2/SiO_2 (OP) composite particles (b).

with a size of 280 nm in the range of 175–450 nm (Fig. 16).

Moreover, PCA of nanocomposites depends on the specific surface of the silica, and the adsorption activity does not depend on its composition, but is determined by it, especially the composition of the surface of the nanocomposite. It is found that the photocatalytic activity in the visible range of the TiO_2/SiO_2 nanocomposite (granules) photosensitized with coproporphyrin I (method 1) exceeds more than 20-fold the activity of the commercial reference sample of "$TiSiO_4$."

ACKNOWLEDGMENTS

This work was partially supported by Russian Foundation for Basic Research (project no. 15-03-01289).

REFERENCES

1. G. Erlikh, *Small Objects—Great Ideas. A Broad View of Nanotechnology* (BINOM. Laboratoriya Znanii, 2012) [in Russian].
2. M. Dadachov, "Novel titanium dioxide, process of making and method of using same," US Patent No. 0171877 (2006).
3. M. Dadachov, "Novel adsorbents and process of making and using same," US Patent No. 0144793 (2006).
4. S. Singh, K. C. Barick, and D. Bahadur, "Functional oxide nanomaterials and nanocomposites for the removal of heavy metals and dyes," Nanomater. Nanotechnol. **3**, 20 (2013).
5. K. E. Engates and H. J. Shipley, "Adsorption of Pb, Cd, Cu, Zn and nitotitanium dioxide nanoparticles: effect of particle size, solid concentration, and exhaustion," Environ. Sci. Pollut., No. 18, 386–395 (2011).
6. P. A. Demina, A. A. Kuz'michev, A. M. Tsybinsky, L. N. Obolenskaya, G. M. Kuz'micheva, E. N. Domoroshchina, and E. V. Savinkina, "Synthesis, characterization and adsorption behavior of Mo(VI) and W(VI) ions on titanium dioxide nanoparticles containing anatase modification," Appl. Nanosci. **4**, 979–987 (2014).
7. P. A. Demina, A. M. Zybinskii, G. M. Kuz'micheva, L. N. Obolenskaya, E. V. Savinkina, and N. A. Prokudina, "Adsorption ability of samples with nanoscale anatase to extract Nb(V) and Ta(V) ions from aqueous media," Crystallogr. Rep. **59**, 430 (2014).
8. G. M. Kuz'micheva, E. N. Domoroshchina, E. V. Savinkina, and L. N. Obolenskaya, "Nanosized titania with anatase structure: synthesis, characterization, applications and environmental effects," in *Titanium Dioxide: Chemical Properties, Applications and Environmental Effects,* Chemical Engineering Methods and Technology (Nova Science, USA, 2014), Chap. 9, pp. 177–227.
9. S. Banerjee, S. C. Pillai, P. Falaras, K. E. O'Shea, J. A. Byme, and D. D. Dionysiou, "New insights into the mechanism of visible light photocatalysis," J. Phys. Chem. Lett. **5**, 2543–2514 (2014).
10. A. Fujishima, K. Hashimoto, and T. Watanabe, *TiO_2 Photocatalysis: Fundamentals and Applications* (BKC, Tokyo, 1999).
11. J. G. Yoon, H. K. Oh, and Y. J. Kwag, "Structural and optical properties of TiO_2-SiO_2 composite films prepared by aerosol-assisted chemical-vapor deposition," J. Korean Phys. Soc. **33**, 699–704 (1998).
12. K. Balachandaran, R. Venckatesh, and R. Sivaraj, "Synthesis of nano-TiO_2-SiO_2 composite using sol-gel method: effect on size, surface morphology and thermal stability," Int. J. Eng. Sci. Technol. **2**, 3695–3700 (2010).
13. A. Nilchi, S. Janitabar-Darzi, and S. Rasouli-Garmarodi, "Sol-gel preparation of nanoscale TiO_2/SiO_2 composite for eliminating of con red azo dye," Mater. Sci. Appl. **2**, 476–480 (2011).
14. K. Balachandran, R. Venckatesh, and R. Sivaraj, "Photocatalytic decomposition of isolan black by TiO_2–SiO_2

core shell nanocomposites," Int. J. Res. Eng. Technol. **2** (9), 46–51 (2013).

15. D. A. Kumar, J. M. Shyla, and F. P. Xavier, "Synthesis and characterization of TiO_2/SiO_2 nanocomposites for solar cell applications," Appl. Nanosci. **2**, 429–436 (2012).
16. L. Pinho, F. Elhaddad, D. S. Facio, and M. J. Mosquera, "A novel TiO_2–SiO_2 nanocomposite converts a very friable stone into a self-cleaning building material," Appl. Surf. Sci. **275**, 389–396 (2013).
17. L. N. Obolenskaya, G. M. Kuz'micheva, E. V. Savinkina, N. V. Sadovskaya, A. V. Zhilkina, N. A. Prokudina, and V. V. Chernyshev, "Influence of the conditions of the sulfate method on the characteristics of nanosized anatase-type samples," Russ. Chem. Bull. **61**, 2049–2055 (2012).
18. J. Canny, "A computational approach to edge detection," IEEE Trans. Pattern Anal. Machine Intelligence **8**, 679–698 (1986).
19. D. S. Tsoukleris, A. I. Kontos, P. Aloupogiannis, and P. Falaras, "Photocatalytic properties of screen-printed titania," Catal. Today **124**, 110–117 (2007).
20. P. Falaras, "Synergetic effect of carboxylic acid functional groups and fractal surface characteristics for efficient dye sensitization of titanium oxide," Sol. Energy Mater. Sol. Cells **53**, 163–175 (1998).
21. J. Zhao, C. Chen, and W. Ma, "Photocatalytic degradation of organic pollutants under visible light irradiation," Top. Catal. **35**, 269–278 (2005).
22. E. V. Savinkina, G. M. Kuzmicheva, and L. N. Obolenskaya, "Synthesis, characterization and photocatalytic properties of η-titania," Int. J. Energy Environ., No. 6, 268 (2012).
23. E. V. Savinkina, L. N. Obolenskaya, G. M. Kuz'micheva, A. V. Dorokhov, and A. Yu. Tsivadze, "A new η-titania-based photocatalyst," Dokl. Phys. Chem. **441**, 224 (2011).
24. E. V. Savinkina, L. N. Obolenskaya, G. M. Kuz'micheva, and A. V. Dorokhov, "Nanosized η-titania-based photocatalyst," Patent RF No. 24697.
25. I. A. Zamilatskov, E. V. Savinkina, A. N. Volov, M. S. Grigor'ev, I. S. Lonin, L. N. Obolenskaya, G. V. Ponomarev, O. I. Koifman, A. S. Kuzovlev, G. M. Kuz'micheva, and A. Yu. Tsivadze, "Synthesis, structures and photosensitizing properties of new porphyrins, Pt(II) and Pd(II)," Macroheterocycles **5**, 308 (2012).
26. J. H. Cai, Y. J. Ye, J. W. Huang, H. C. Yu, and L. N. Ji, "Synthesis, characterization and visible-light photocatalytic activity of TiO_2–SiO_2 composite modified with zinc porphyrins," J. Sol-Gel Sci. Technol. **62**, 432–440 (2012).
27. A. Gainanova, G. Kuz'micheva, E. Kabachkov, and A. Zybinskiy, "Preparation, characterization, photocatalytic and adsorption properties of samples with nano-η-TiO_2," in *Proceedings of the 12th International Conference on Crystal Chemistry of Intermetallic Compounds, Lviv, Ukraine, Sept. 22–26, 2013*, p. 183.

Translated by Sh. Galyaltdinov